Progress In Electromagnetics Research C, Vol. 131, 103–117, 2023

Analyses of Absorbing Boundary Conditions in 2D FDTD Simulations for Electromagnetic Wave Propagation in Anisotropic Ionosphere

Md Yusoff Siti Harwani[1, *] **and Tiem Leong Yoon**[2]

Abstract—Implementing appropriate absorbing boundary conditions (ABCs) in finite-difference time-domain (FDTD) simulations is essential. Optimal ABCs can help minimize or even eliminate spurious reflections in simulations involving waves impinging on the edges of simulation grid boundaries. In this work, 2D FDTD code facilitating ABCs were implemented and incorporated under plug-and-play conditions. Using this FDTD code, two different types of ABCs were evaluated: a differential ABC and a perfectly matched layer (PML) for the anisotropic medium of the ionosphere. Furthermore, numerical experiments were conducted to examine the efficiencies of both these ABCs; a total of $n = 2000$ iterations were adopted under grid conditions of 120 in the y-direction, 600 in the x-direction of spatial step, and $\Delta x = 1000\,\text{km}$. Additionally, n was set as a time-equivalent variable in these simulations. For the interval $\Delta x = 1\,\text{km}$ between any two adjacent grid points, active conditions for the grid simulation were determined within 120 km in the y-direction (vertical) and 600 km in the x-direction (horizontal). Furthermore, numerical experiments revealed that the PML platform yielded excellent efficiency compared to the differential ABC.

1. INTRODUCTION

When finite-difference time-domain (FDTD) numerical analyses are employed for time-stepping Maxwell's equations, employing absorbing boundary conditions (ABCs) is crucial, particularly to account for the absorption of electromagnetic waves as they propagate through media. Prior to the introduction of the perfectly matched layer (PML), ABCs were typically implemented using analytical schemes [1, 2] or alternative methods such as differential ABC approach [3].

However, the PML scheme is preferred over these conventional methods because it is extensive and efficient for homogeneous, inhomogeneous, linear, nonlinear, isotropic, and anisotropic domains. The most popular PML method is the approach proposed by Berenger, which entails splitting electric and magnetic fields [4]. Notably, this technique minimizes the reflections from a boundary by imposing fictitious conductivities in both these fields. In further investigations based on the work conducted by Berenger, the unsplit field of a PML was introduced to anisotropic media with complex permittivities and permeabilities. The numerical stability of this method is achieved by fulfilling the requirement of Courant stability factor. Berenger's work has also been examined by several other researchers [5–8]. In addition, numerical stability at high frequency can also be achieved by applying semi-analytical approach in derivation process, as shown in [9] and [10].

For a linear, isotropic, non-dispersive medium with rectangular coordinates and space-varying characteristics, developing a 2D FDTD numerical code is not complicated. However, for anisotropic

---

Received 23 November 2022, Accepted 10 March 2023, Scheduled 20 March 2023

* Corresponding author: Md Yusoff Siti Harwani (aeharwani@usm.my).

[1] School of Aerospace Engineering, Universiti Sains Malaysia Engineering Campus, Penang 14300, Malaysia. [2] School of Physics, Universiti Sains Malaysia, Penang 11800, Malaysia.

(dispersive) media such as ionosphere, the FDTD numerical algorithm required for robust outputs might rely on nontrivial conditions. This is primarily attributed to the inherent numerical complexity of Maxwell's equations for such media [11–15]. There is sphere waves scattering method applicable to a problems such as ionosphere, known as Watson Transformation, used to compute electric field of the Earth, mentioning the complexity of the computation for the spherical using extreme low frequency (ELF) waves [16, 17]. Furthermore, the variations in the physical properties of the ionosphere as a function of altitude also contribute to this numerical complexity. To address the complexity issue, this work introduces a 2D FDTD algorithm for ABCs, with the aim of modeling the propagation of electromagnetic (EM) waves under anisotropic and inhomogeneous ionospheric conditions. Both types of ABCs are investigated for their effectiveness by executing a numerical simulation and then examining the relative error acquired in each case.

2. METHODOLOGY

Here, the FDTD algorithm was implemented under inhomogeneous and anisotropic conditions for the time-stepping of a 2D spherical EM wave in a rectangular coordinate system. The algorithm used was adapted from the work of Chen et al. [18] and expressed as a functional example for modeling a similar system using FDTD simulations. This is also termed as J-E convolution. This algorithm was selected based on the results obtained via tests conducted using a trial-and-error approach and to other previous numerical schemes for implementing FDTD simulations under anisotropic (dispersive) conditions. A dispersive medium is either field-, direction-, or frequency-dependent based on its electric and magnetic properties. Furthermore, the adoption of the J-E convolution scheme was tested thoroughly, and a reliable output was obtained after extensive pretesting [19]. As a result, Maxwell's equations for wave propagation in an anisotropic dispersive medium can be expressed as follows:

$$\nabla \times E = -\mu_0 \frac{\partial H}{\partial t}, \tag{1a}$$

$$\nabla \times H = \varepsilon_0 \frac{\partial E}{\partial t} + J, \tag{1b}$$

$$\frac{dJ}{dt} + \nu J = \varepsilon_0 \omega_p^2 E + \omega_b \times J, \tag{1c}$$

where J is the electric current density in A/m^2; E is the electric field intensity, in V/m; H is the magnetic field intensity, in V/m; and ε_0 and μ_0 are the permittivity and permeability of the free space, respectively [20]. The numerical solution for Maxwell's equations is expressed in terms of the transverse magnetic (TM) mode, based on the E_z, H_x, and H_y components of the electromagnetic field. These field components are treated as functions of the temporal variable (t) and 2D spatial coordinates (x, y). Assuming that the incident wave is uniform and independent of the spatial variable z, B_0 is parallel to the z-axis with angular frequencies of $\omega_{bx} = 0$, $\omega_{by} = 0$ and $\omega_{bz} = \omega_b$. Thus, Equation (1c) can be expressed as

$$\frac{dJ_z}{dt} = \varepsilon_0 \omega_p^2 E_z - \nu J_z. \tag{2}$$

Thereafter, Equation (2) is Laplace transformed in the s-domain using the following expressions:

$$\frac{dJ\left(t\right)}{dt} \quad \Leftrightarrow \quad sJ\left(s\right) - J_0 \tag{3}$$

$$\varepsilon_0 \omega_p^2 E\left(t\right) \quad \Leftrightarrow \quad \varepsilon_0 \omega_p^2 E\left(s\right) \tag{4}$$

$$\Omega J\left(t\right) \quad \Leftrightarrow \quad \Omega J\left(s\right) \tag{5}$$

In the s-domain, Equation (3) becomes

$$J\left(s\right) = \left(sI - \Omega\right)^{-1} J_0 + \varepsilon_0 \omega_p^2 \left(sI - \Omega\right)^{-1} E\left(s\right) \tag{6}$$

where I denotes an identity matrix and $\Omega = \begin{pmatrix} -\nu & -\omega_b \\ \omega_b & -\nu \end{pmatrix}$. The inverse matrix $(sI - \Omega)^{-1}$ is expressed in terms of

$$A = (sI - \Omega)^{-1} = \frac{1}{(s+\nu)^2 + \omega_b^2} \begin{pmatrix} s+\nu & -\omega_b \\ \omega_b & s+\nu \end{pmatrix}. \tag{7}$$

Equation (6) can be rewritten as

$$J(s) = A(s)\, J_0 + \varepsilon_0 \omega_p^2\, A(s)\, E(s). \tag{8}$$

Using the Laplace transform of Equation (8) for the t-domain, $J(t)$ becomes

$$J(t) = A(t)\, J_0 + \varepsilon_0 \omega_p^2\, K(t), \tag{9}$$

where

$$A(t) = e^{-\nu t} \begin{pmatrix} \cos\omega_b t & -\sin\omega_b t \\ \sin\omega_b t & \cos\omega_b t \end{pmatrix} \tag{10}$$

and

$$K(t) = A(t) * E(t). \tag{11}$$

Here, J_z is only dependent on ν and ω_p and independent of ω_b [15].

In the case of $\omega_{bx} = 0$ and $\omega_{by} = 0$, the FDTD iteration of Equation (2) can be acquired into the following form (Δt) with the size of the time step, n:

$$J_z\Big|_{i,j}^{n+\frac{1}{2}} = e^{-\nu\Delta t}\, J_z\Big|_{i,j}^{n+\frac{1}{2}} + \varepsilon_0 \omega_p^2\, \Delta t e^{\frac{-\nu\Delta t}{2}}\, E_z\Big|_{i,j}^{n}. \tag{12}$$

ω_p in Equation (12) is defined by the electron density N_e. The relationship between ω_p and N_e is represented as in Equation (13):

$$\omega_p = \sqrt{\frac{N_e(h)\, e^2}{m_e \varepsilon_0}}. \tag{13}$$

The fields in the TM mode, that is E_z, H_x, and H_y, can be obtained by discretizing Equation (1):

$$H_x\Big|_{i,j+\frac{1}{2}}^{n+\frac{1}{2}} = D_{ax}(i,j) * H_x\Big|_{i,j+1/2}^{n-1/2} - D_{bx}(i,j) * \left[E_z\Big|_{i,j+1}^{n} - E_z\Big|_{i,j}^{n}\right], \tag{14a}$$

$$H_y\Big|_{i+1/2,j}^{n+1/2} = D_{ay}(i,j) * H_y\Big|_{i+1/2,j}^{n-1/2} + D_{by}(i,j) * \left[E_z\Big|_{i+1,j}^{n} - E_z\Big|_{i,j}^{n}\right] \tag{14b}$$

$$E_z\Big|_{i,j}^{n} = C_{ax}(i,j) * E_z\Big|_{i,j}^{n} - J_z\Big|_{i,j}^{n+1} + C_{bx}(i,j)\left[H_y\Big|_{i+\frac{1}{2},j}^{n+\frac{1}{2}} - H_y\Big|_{1-\frac{1}{2},j}^{n+\frac{1}{2}} - H_x\Big|_{i,j+\frac{1}{2}}^{n+\frac{1}{2}} - H_x\Big|_{i,j-\frac{1}{2}}^{n+\frac{1}{2}}\right], \tag{14c}$$

$$J_z\Big|_{i,j}^{n+1/2} = e^{-\nu\Delta t}\, J_z\Big|_{i,j}^{n+1/2} + \varepsilon_0 \omega_p^2 \Delta t e^{\frac{-\nu\Delta t}{2}}\, E_z\Big|_{i,j}^{n}. \tag{14d}$$

where C_{ax} and C_{bx} are the coefficients of the electric field, and $D_{ax}, D_{bx}, D_{ay}, D_{by}$ are the coefficients of the magnetic field, which are defined as

$$C_{ax}(i,j) = \frac{\left(1 - \dfrac{\sigma\Delta t}{2\varepsilon_0}\right)}{\left(1 + \dfrac{\sigma\Delta t}{2\varepsilon_0}\right)} \tag{15}$$

$$C_{bx}(i,j) = \frac{\left(\dfrac{\Delta t}{\varepsilon_0 \Delta}\right)}{\left(1 + \dfrac{\sigma\Delta t}{2\varepsilon_0}\right)} \tag{16}$$

$$D_{ax}(i,j) = D_{ay}(i,j) = \frac{\left(1 - \dfrac{\sigma^*\Delta t}{2\mu_0}\right)}{\left(1 + \dfrac{\sigma^*\Delta t}{2\mu_0}\right)} \tag{17}$$

$$D_{bx}\left(i,j\right) \;=\; D_{by}\left(i,j\right)=\frac{\left(\dfrac{\Delta t}{\mu_0\Delta}\right)}{\left(1+\dfrac{\sigma^*\Delta t}{2\mu_0}\right)} \tag{18}$$

where $\sigma = \sigma^*$ denotes the conductivity of the material. Under this condition, σ is applied to the electric field element, whereas σ^* is applied to the magnetic field element. Further, $\Delta = \Delta x = \Delta y$ is the spatial width, expressed in terms of a fraction of the wavelength λ as $\Delta = \lambda/N$. N is denoted as either a positive real or positive integer n, and (i, j) represents the temporal and spatial discretization indices, respectively. The convergence of the FDTD simulation (where the time-stepping evolution of the EM profile remains finite and stable even after several steps) depends on the choice of Δt, which must be sufficiently small to ensure that the wave has adequate time to propagate through the spatial grid. This requirement is also known as the Courant (Friedrich) stability factor [20]. The limit of the time increments to ensure stability in the 2D FDTD simulation can be expressed as

$$\Delta t \le \frac{1}{c_0\sqrt{\dfrac{1}{\left(\Delta x\right)^2}+\dfrac{1}{\left(\Delta y\right)^2}}} \tag{19}$$

where c_0 is the speed of light. We define the Courant-Friedrich-Lewis (CFL) number as

$$\mathrm{CFL} = c_0\Delta t\sqrt{\frac{1}{\left(\Delta x\right)^2}+\frac{1}{\left(\Delta y\right)^2}} \tag{20}$$

and the stability condition may be written as

$$\mathrm{CFL} < 1. \tag{21}$$

For simplification, the time increment to satisfy the CFL stability requirement in 2D can be written as

$$\Delta t = \frac{\Delta}{2c_0}. \tag{22}$$

In this study, the wave source for the FDTD modeling was implemented by generating a point sinusoidal source at the grid site $i = 2$, $j = 2$, as

$$E_z\,\big|_{i,j}^{n} = A_0 \sin\left(2\pi f_0 n\Delta t\right), \tag{23}$$

where f_0 is the frequency (30 kHz), and A_0 is the amplitude (10 m). At the source of the grid site $i = 2$, $j = 2$, E_z is equal to 3.09017 V/m, and n is equal to 2000.

The wave propagation cannot be simulated infinitely in an active grid; hence, it must be terminated at the edges. Furthermore, the mechanism of ABC is based on dampened fields propagating into an absorbing medium. Thus, in a typical FDTD simulation, the ABC must be set up on all edges enclosing the active simulation grid.

In this study, two types of ABCs have been employed to develop the FDTD code. One is the first-order ABC [2], and the other is PML ABC, as proposed by Berenger [21]. These two different types of ABCs are implemented to investigate the best method for the time-stepping of EM fields in the anisotropic ionosphere and examine the effectiveness of both approaches. As shown in Figure 1, the 2D computational grid of the present FDTD modeling has dimensions of 600 km × 120 km along the x- and y-directions. This modeling is composed of two regions which are the unshaded area known as the active simulation grid and the shaded stripe area at the edges where the ABC scheme is to be implemented. Generally, the stripes are commonplace on all sides and vary depending on the parameter used for the ABC scheme.

The extensive simulation while the ABC in the anisotropic environment is implemented, in the case of ionospheric studied in this work, shows that the reflection from the boundary is not suppressed entirely but occurs only to a certain extent. Furthermore, the quantitative performance of two different types of ABC used in this work is discussed below.

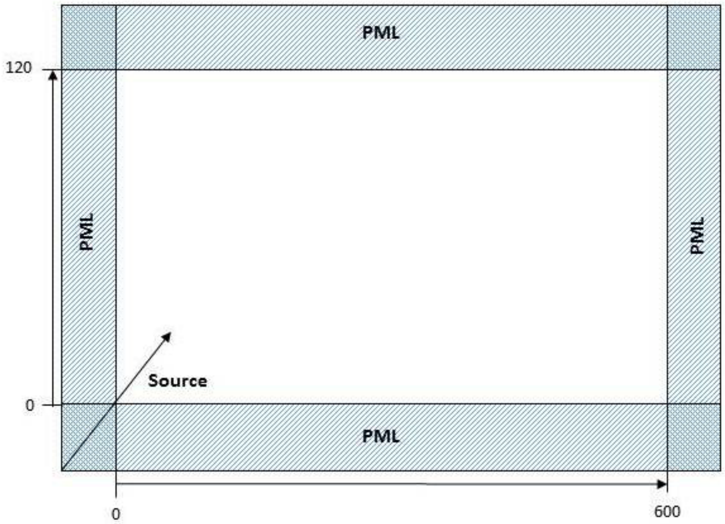

Figure 1. Two-dimensional computational grids for wave propagation. The shaded stripes along the edges are grid layers where ABC is to be implemented.

For the ABC mechanism, the electric fields travel within the one-time step. In contrast, the magnetic field travels at halftime steps, so the alteration of two-time steps is implemented to terminate the propagated wave. Equation (24) shows the proposed method for how the ABC is to be implemented.

$$E_z\,|_{0,j}^{n+1} = E_z\,|_{1,j}^{n} \tag{24a}$$

$$E_z\,|_{ie,j}^{n+1} = E_z\,|_{ie-1,j}^{n} \tag{24b}$$

$$E_z\,|_{i,0}^{n+1} = E_z\,|_{i,1}^{n} \tag{24c}$$

$$E_z\,|_{i,je}^{n+1} = E_z\,|_{i,je-1}^{n} \tag{24d}$$

where $i = 1, 2, 3, ..., ie$, $j = 1, 2, 3, ..., je$, $ie = 600$, and $je = 120$. By implementing this condition, the wave will be absorbed by the termination at the edges.

The second type of ABC used in this work is the PML ABC which was initially proposed by Yee [22]. The PML absorber layer is introduced with a damping profile located at the edge of the simulation grid, which can be characterized spatially by various functions, which constitute of a few independent variables such as conductivity, PML thickness, and reflection coefficient. To improve the performance of wave absorption, which covers a large range of frequencies, Rickard and Georgieva have proposed to introduce conductivity into the function σ_k which varies in a stepwise manner from one spatial grid point, k, to the next spatial grid [23]. It is noted that in the 2D simulation grid, k is referred to either as spatial i in the x-direction or j in the y-direction index. This structure will enable the development of loss behavior at a different rate when waves (which incident from the active simulation grid section) propagate into layers. Furthermore, to achieve an almost reflection-free scenario, Rickard and Georgieva have recommended a PML conductivity function which consists of a loss factor, which is represented as $\alpha_k(\rho)$ in Eq. (25) that assumes the form of

$$\sigma_k\left(\rho\right) = \sigma_{\max}\left(\frac{\rho_k}{\delta_k}\right)^{k+\beta} \tag{25a}$$

$$\alpha_k\left(\rho\right) = 1 + \varepsilon_{\max}\left(\frac{\rho_k}{\delta_k}\right)^{k} \tag{25b}$$

The user-defined parameter, $\sigma_{\max}$, is used for controlling the attenuation of propagating waves, as in Equation (26),

$$\sigma_{\max} = -\left[\left(h + \beta + 1\right)\varepsilon_0 \cdot c_0 \cdot \ln R_0 / \left[2/\delta_k\right]\right] \tag{26}$$

where R_0 is the reflection coefficient, δ_k the thickness of the PML in the grid index by k, h the user-defined rate of growth, β the user-defined difference in the exponent rates, $\varepsilon_{\max}$ the user-defined parameter to control the rate of evanescent mode attenuation, ρ_k the depth in PML (measured orthogonally from the boundary separating the active simulation grid and the PML), and c_0 the speed of light.

Table 1 shows the range for each parameter, as proposed by Rickard and Georgieva [23].

Table 1. PML absorber parameters and their range.

Parameter	User-defined range	Proposed value
$\boldsymbol{R_0}$	$\left[10^{-2}, 10^{-12}\right]$	10^{-5}
$\boldsymbol{\rho_k}$	$0 \leq \rho_k \leq \delta_k$	25
$\boldsymbol{\varepsilon_{\max}}$	$[0, 10]$	0
h	$[2, 6]$	4
$\boldsymbol{\beta}$	$[-3, 3]$	0

In this study, a PML strip was added at the edge of the simulation grid, with a total width of 25 cells (each cell had a width of δ_k). The conductivity σ_k was incorporated in the FDTD code via the medium coefficient, as shown below:

$$C_{ax}(i,k) = \frac{\left(1 - \dfrac{\sigma_k \Delta t}{2\varepsilon_0}\right)}{\left(1 + \dfrac{\sigma_k \Delta t}{2\varepsilon_0}\right)}, \tag{27a}$$

$$C_{bx}(i,k) = \frac{\left(\dfrac{\Delta t}{\varepsilon_0 \Delta}\right)}{\left(1 + \dfrac{\sigma_k \Delta t}{2\varepsilon_0}\right)}, \tag{27b}$$

$$D_{ax}(i,k) = D_{ay}(k,j) = \frac{\left(1 - \dfrac{\sigma_k^* \Delta t}{2\mu_0}\right)}{\left(1 + \dfrac{\sigma_k^* \Delta t}{2\mu_0}\right)}, \tag{27c}$$

$$D_{bx}(i,k) = D_{by}(k,j) = \frac{\left(\dfrac{\Delta t}{\mu_0 \Delta}\right)}{\left(1 + \dfrac{\sigma_k^* \Delta t}{2\mu_0}\right)}, \tag{27d}$$

where $\sigma_k^* = \sigma_k$.

Table 2 summarizes the values of the FDTD and PML parameters used in the 2D simulation under the TM mode.

For comparing the effectiveness of the differential ABC and PML technique, the electric field, E_z, is investigated at six different locations in the active simulation region, designated as A, B, C, D, E, and F, as shown in Figure 2. All these points are selected randomly for the intention of observation.

In this work, the relative error calculation is implemented to address the accuracy of the measurement quantitatively. The relative error is denoted as the absolute error divided by the magnitude of the exact value, which implies the magnitude of the difference between the exact value and its approximation. It is noted that the lowest relative error is acknowledged as the most excellent accuracy. Nonetheless, at each site which the calculation implies, the relative error at the given instant time-step

Table 2. Summary of the values for FDTD and PML parameters.

Parameters	Value
Dimensions of active simulation region	$600 \times 120\Delta x$
No. of PML layers	25
EM source	2-D sinusoidal point source
Source location	$i = 2$, $j = 2$
Frequency, f_0	30 kHz
Courant factor for numerical stability, CLF	$\Delta t = 1.6 \times 10^{-6}$ $\Delta x = \lambda/10$ $\mathrm{CLF} = c_0 \Delta t/\Delta x$
Numerical dispersion	1 km
Relative permittivity, ε_0	1
Relative permeability, μ_0	1

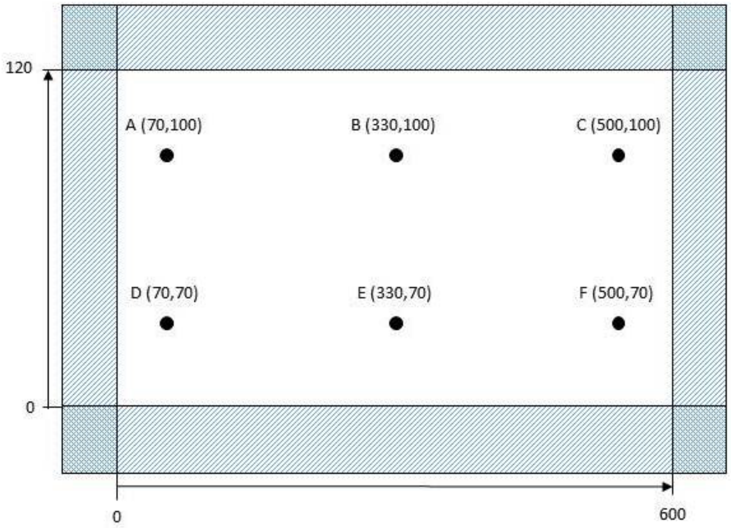

Figure 2. The location of the sites in which the relative error of the electric field is accessed.

n is measured using Equation (28) which is written below:

$$\mathrm{Rel.\,error}\big|_{i,j}^{n} = \left| E_z\big|_{i,j}^{n} - E_{ref}\big|_{i,j}^{n} \right| \Big/ \left| E_{ref,\max}\big|_{i,j} \right|, \tag{28}$$

where E_{ref} the reference value of an electric field at a probing site with time-step n in a reference domain is within the extra-large grid of the dimension 1000×360. Moreover, the value $E_{ref}|_{i,j}^{n}$ refers to the value of E_z which was measured independently in the reference domain at time n when reflections from the boundaries have not arrived at (i, j) during the time $E_z|_{i,j}^{n}$ (which may contain contamination from reflection from the edges) while being recorded. Furthermore, $E_{ref}|_{i,j}^{n}$ is designed to be clear from contamination located at the edge-reflected waves throughout the entire process of the simulation. $E_{ref,\max}$ is the maximum amplitude of the electric field from the reference solution E_{ref}, which was observed during the time-stepping time of interest.

Both types of ABC which were elaborated in the previous paragraph are investigated thoroughly for their effectiveness by executing a numerical simulation and then examining the relative error acquired in each case. Last but not least, the relative error is measured for each time step n for PML by varying the cell number for 5, 10, 15, 20, and 25. Finally, the outcome of the numerical experiment is described comprehensively, and the effectiveness of both ABC methods is described quantitatively.

3. RESULTS AND DISCUSSION

3.1. Numerical Experiment with ABCs

The first part of the numerical experiment to investigate the effectiveness of the ABCs entailed propagating a 2D spherical wave from a point source located at the origin. The EM waves were then time-stepped sequentially in the active simulation grid. Next, the electric field component E_z was probed and numerically measured at the selected sites: A, B, C, D, E, and F. The locations of the probes were designated as A($i = 70$, $j = 100$), B($i = 330$, $j = 100$), C($i = 500$, $j = 100$), D($i = 70$, $j = 70$), E($i = 330$, $j = 70$), and F($i = 500$, $j = 70$), as shown in Figure 2. Furthermore, in Figure 3, the simulated EM wave patterns at $n = 2000$ steps are visualized.

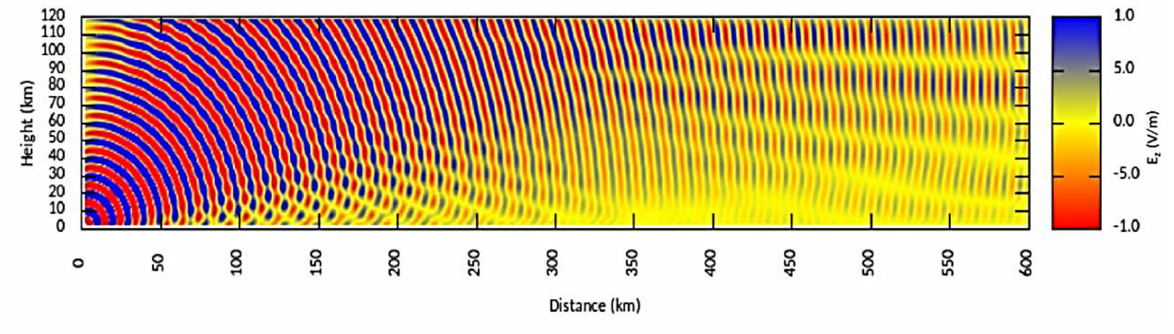

Figure 3. E_z field components for ABC after 2000 steps.

The relative errors obtained at these points for the exact step n were calculated using Equation (28). Figure 4 shows the variations in the relative error with an increase in the simulated time steps for sites A, B, C, D, E, and F. In general, for each site, Figure 4 indicates that the relative errors are suppressed below a value of 1.00. These results suggest that the reflected waves are significantly suppressed after interacting with the boundaries, as compared with the incident waves, which are partially absorbed. Furthermore, when the EM waves pass through a different site immediately before the interference of the reflected waves from the boundaries, the relative errors remain at zero. This phenomenon is depicted in the subfigures of Figure 4.

Moreover, when the reflected waves from the boundaries reach a specific site at any time, interference occurs due to the waves originating from the source or the surroundings. This is presented in Figure 4 in terms of the deviation from zero or the constant trend of each relative error with respect to the time step. The initial period of the deviation from zero or the flat trend in the graph is indicative of the arrival of non-absorbed reflected waves from the boundaries. Given that the probing site is located far from the sources, the EM waves from the source or those reflected from the boundaries arrive much later. Hence, the deviation at the farthest probing site, as compared with the nearest probing site from the sources, results in the deviation from the zero values or the flat trend into relative errors values occurring much later. As such, each site has location-dependent “on-set instance” characteristics, with certain sites presenting earlier deviations than the other sites. All the expected features were designed in the numerical experiment to probe the relative errors and examine the inefficiency of the ABCs, considering the absorption of EM waves during their interaction with the boundaries.

From Figure 4, it can be observed that the relative errors with respect to the time step for all probing sites typically begin at zero or initially present flat trends; this corresponds to the absence of interference caused by unabsorbed waves from the boundaries. Thereafter, when these interference waves arrive at the probe region, the graph gradually deviates from zero or the flat trends; this occurs in addition to an array of short transitions of approximately 40–150 simulation steps, denoted as “steady state.” In this region, the relative errors typically oscillate periodically at the frequency of the EM wave, and the amplitude either increases or varies over an extended period. Subsequently, the steady state undergoes a transition to one with smaller or larger relative errors. Fundamentally, the amplitude of the relative errors in the steady-state region for every point in the simulation grid can be examined.

However, this is significantly time-consuming; this can be reduced to a few representative sites, as realized in this work. Moreover, the measured maximum amplitude of the relative errors in the steady-state region is a conventional indicator of the accuracy of FDTD simulations for EM wave propagation in the ionosphere.

For site A, the simulated data showed that the relative errors reached a periodically steady state after 1350 steps, resulting in an almost constant trend below 4×10^{-1}. At site B, the measured relative errors decreased after 950 simulation steps and were less than 2×10^{-1}. At site C, the amplitude of the relative errors initially appeared exceeding 4×10^{-1}. Subsequently, after approximately 1430 steps, the amplitude decreased to less than 3×10^{-1}. However, the relative errors at site D were similar to those at site A, and a steady-state condition was reached after 1350 steps. Furthermore, at site E, the reflection errors increased after approximately 1740 time-steps; the steady-state amplitude was less than 4×10^{-1}. Lastly, the errors at site F increased from zero after 1650 steps. This indicates that the highest amplitude of the steady-state errors across all sites is 4.6×10^{-1}.

The overall relative errors for each site were combined to extrapolate the variations in the interference from sites A to F, as shown in Figure 4(g). It was noted that the relative errors at sites D and C were comparable; however, site D is the closest to the point source, whereas site C is further away from the source and closer to the reflecting edges at the top corner. The relative errors at site

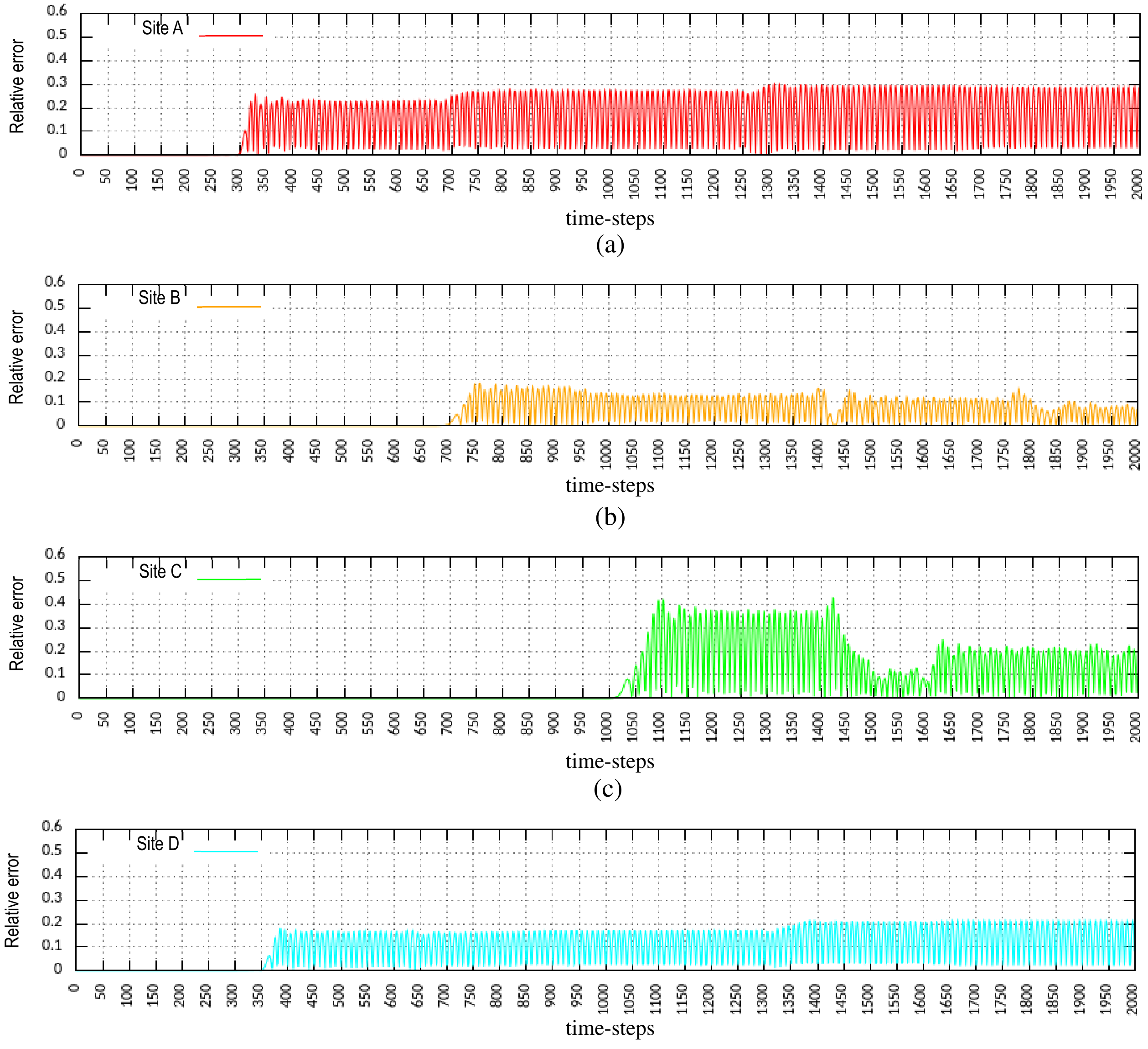

(a)

(b)

(c)

(d)

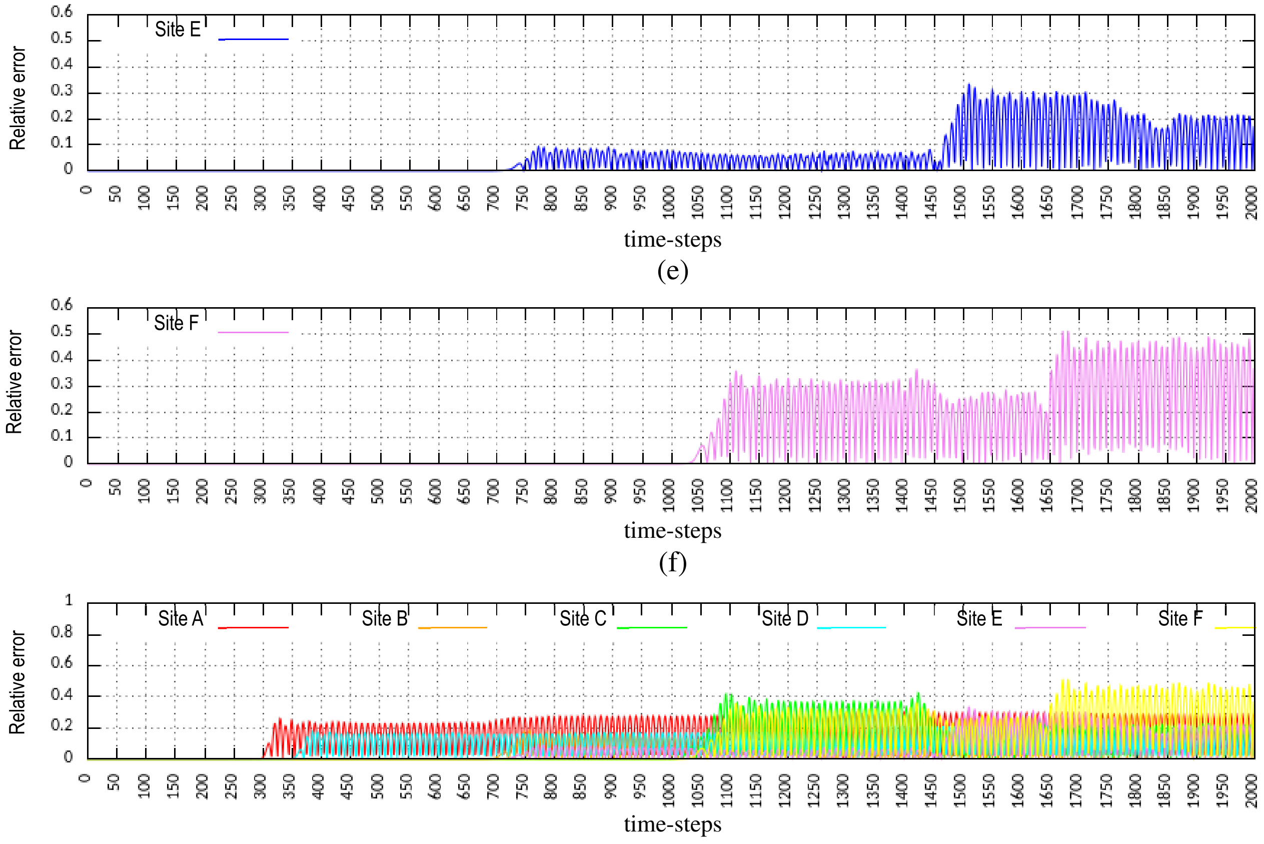

(e)

(f)

(g)

Figure 4. (a) Relative errors at site A within 2000 time-steps using ABC. (b) Relative errors at site B within 2000 time-steps using ABC. (c) Relative errors at site C within 2000 time-steps using ABC. (d) Relative errors at site D within 2000 time-steps using ABC. (e) Relative errors at site E within 2000 time-steps using ABC. (f) Relative errors at site F within 2000 time-steps using ABC. (g) Relative errors at sites A, B, C, D, E and F within 2000 time-steps using ABC.

C are larger owing to the pronounced reflections from the top-right corner, as compared with those at site D.

Furthermore, considering the case wherein waves are absorbed in the boundary under the ABC in the absence of the PML, by implementing the time step, Δt, from Equation (22), the typical field travelling at the speed of light, c_0, can be investigated within one time-step. Thus, the field only travels across half a cell. Hence, to ensure that the field travels across one entire cell, the two-time step condition is crucial. Additionally, under anisotropic conditions in the presence of a dielectric, the propagation speed is not equal to the speed of light, c_0. This causes extensive reflections and high relative errors.

Most importantly, based on the relative error graphs obtained from the probing sites, a constant amplitude of the relative errors is obtained from the simulated EM propagation; this originates from the inefficiency of the ABC employed. The maximum amplitude was less than approximately 0.5 for the entire simulation with $n_{\max} = 2000$, even though the EM propagation oscillated periodically, as shown in Figure 4(g). This trend appears as a desirable steady-state region wherein the relative error does not increase beyond the critical value of 1.0 over one time-step. Therefore, the trend is predicted to be maintained, even for larger values of $n_{\max}$. This, in turn, indicates that the numerical errors in the FDTD code for EM propagation in the ionosphere are capped. Moreover, this ensures that the numerical errors do not increase beyond uncontrollable limits, given that the waves propagate within time steps, even when the order of the simulation period $n_{\max}$ is set to 10^3 or less.

3.2. Numerical Experiment with Perfectly Matched Layer (PML)

This subsection details the outcomes of the numerical experiment conducted to investigate the efficiency of the ABC using the PML method; this experiment was based on the technique proposed by Berenger [21].

The setup for this experiment is similar to that for the differential ABC method. However, in this case, the active simulation grid was surrounded by a PML layer with a width of $w = N_{\mathrm{PML}}\Delta x$, where Δx denotes a spatial grid. To investigate efficiency, the thickness of the PML was varied by adjusting N_{PML}.

Figure 5 illustrates the simulated EM wave for 2000 steps under a PML thickness of $w = 25\Delta x$; the PML, in this case, can be considered to have a thickness of $N_{\mathrm{PML}} = 25$ cells.

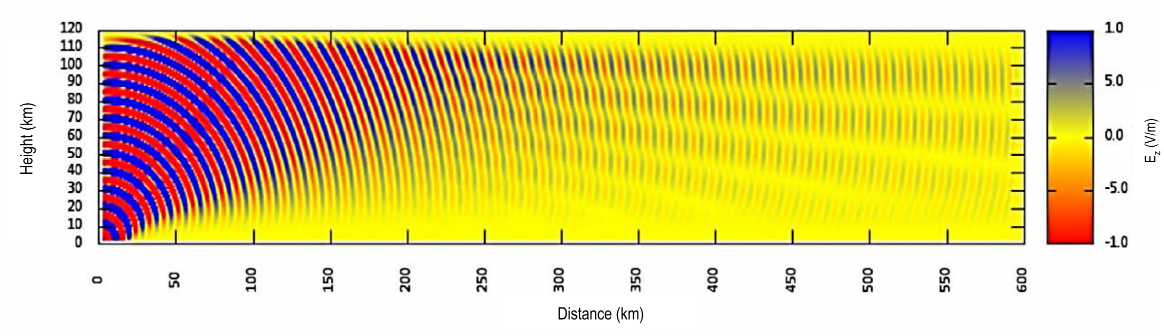

Figure 5. E_z field component for 25 cells of PML after $n = 2000$ steps.

Figures 6(a)–(f) show the collective relative error for the field component E_z, as probed at different sites, with N_{PML} set to 25. Figure 6 shows the extreme suppression behavior of the relative errors at sites A and D. Moreover, these relative errors are less than the critical value of 1.00 for all cases, similar to the previous numerical experiments with the differential ABC method. Moreover, observations performed at sites B and E revealed that the relative errors reached a steady-state condition after 730 steps and were also less than 3×10^{-1}. At sites C and F, the steady-state region of the relative errors featured relatively high values of 4.3×10^{-1} and approximately 5.5×10^{-1}, respectively. It should be noted that the relative errors obtained from site F have the highest values, as compared with those from the other sites for differential ABC and PML in the condition of $N_{\mathrm{PML}} = 25$.

In Figure 6(g), the relative errors with respect to the time steps for all sites are merged to obtain descriptive information. For this purpose, the PML was set to $N_{\mathrm{PML}} = 25$. Furthermore, in Figure 6(g), site F shows the highest relative errors, whereas sites A and D are the most suppressed because both these sites are located farthest from the PML edges.

Typically, in the differential ABC numerical experiment, the thickness parameter cannot be adjusted to alter performance. However, under the PML method, the effect of varying the PML layer thickness, N_{PML}, on the suppression of relative errors has not been elucidated. Hence, the performance of the PML as a function of N_{PML} was investigated in this study.

3.3. Performance of PML with Varying Thickness

A numerical study was performed by varying the thickness N_{PML} as 5, 10, 15, 20, and 25 in order to investigate the efficiency of the PML. This was aimed at determining whether increasing the thickness leads to greater suppression of the relative errors. Moreover, the relative error in E_z was only measured at site F, which is located at $i = 500$, $j = 70$. Site F was selected for this purpose because the relative errors at this location were the largest under both the ABC schemes. These errors can be interpreted as the maximum possible errors in the proposed FDTD simulation. Nevertheless, the actual global relative errors in the FDTD simulation were expected to be less than the conservative errors measured at site F. Figure 7 presents the relative errors at site F for 5, 10, 15, 20, and 25 cells over 2000 time-steps.

At site F, for $N_{\mathrm{PML}} = 5$, the steady-state condition was observed after 1790 time-steps, with a relative error of approximately 1.2. Further, a smaller relative error of approximately 1 was noted for $N_{\mathrm{PML}} = 10$, where the steady-state condition was reached after 1650 time-steps. Moreover, as N_{PML} was increased to 15, 20, and 25, the relative errors gradually decreased to 8×10^{-1}, 7×10^{-1}, and 6×10^{-1}, respectively.

Figure 8 summarizes the performance of the FDTD code in terms of investigating the error absorption when using the PML for different values of 6×10^{-1} in the ionospheric medium. Overall, the graph indicates a slight reduction in the largest steady-state relative error as N_{PML} increases.

Comparatively, similar results were obtained at site F for the PML, and differential ABC approaches in terms of the largest steady-state region, where the error amplitude was 6×10^{-1}. By contrast, on average the results for the other sites, the overall relative error when using the PML was lower than that for the differential ABC method. Notably, the errors at certain sites were significantly suppressed under the PML approach. However, site-specific suppression was not detected for the differential ABC approach.

Considering site-specific error reduction, the PML method was determined to be superior to the differential ABC method. However, to confirm this superiority of the PML method, further evidence is necessary. This can be realized by conducting comprehensive investigations beyond the numerical

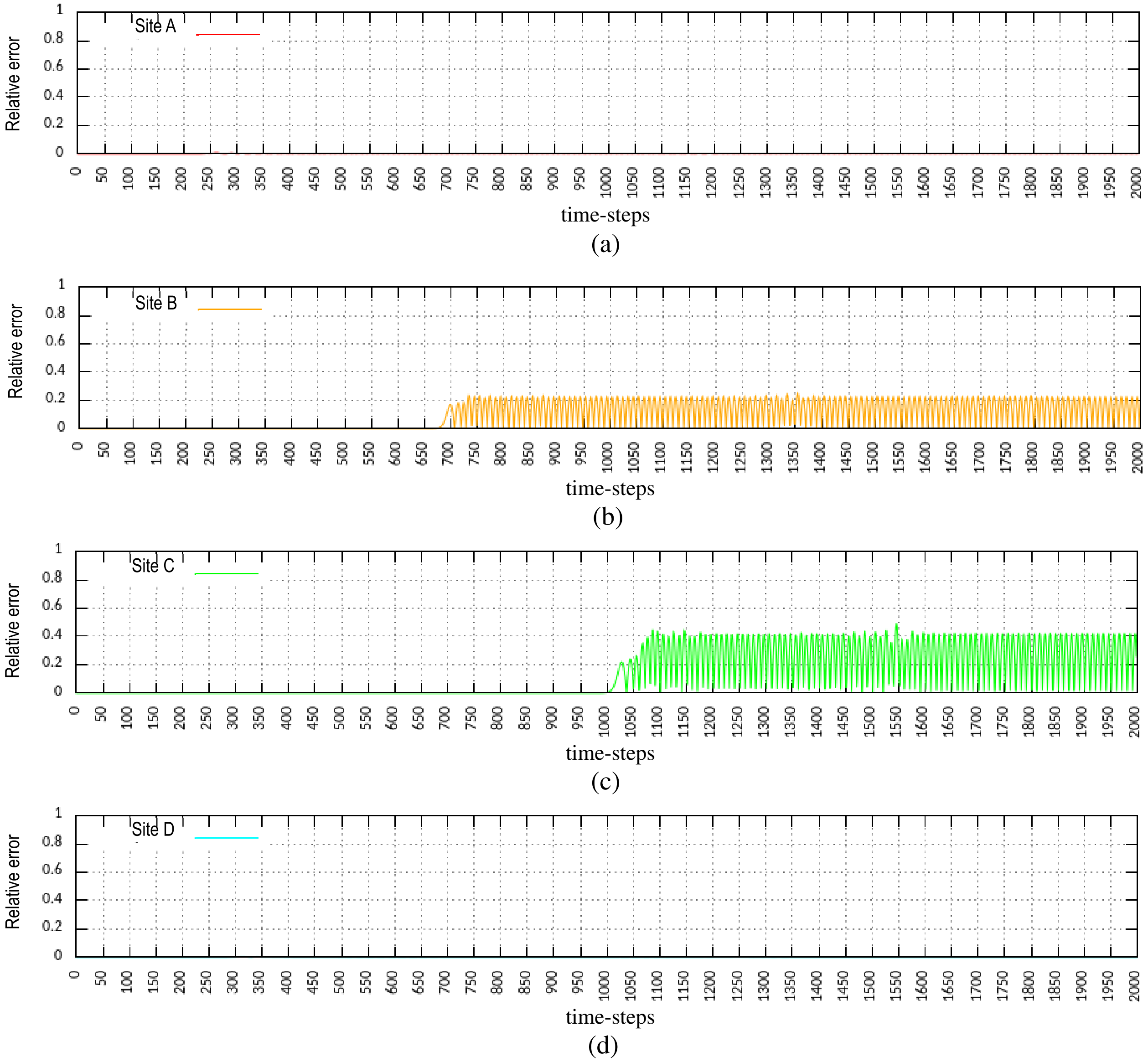

(a)

(b)

(c)

(d)

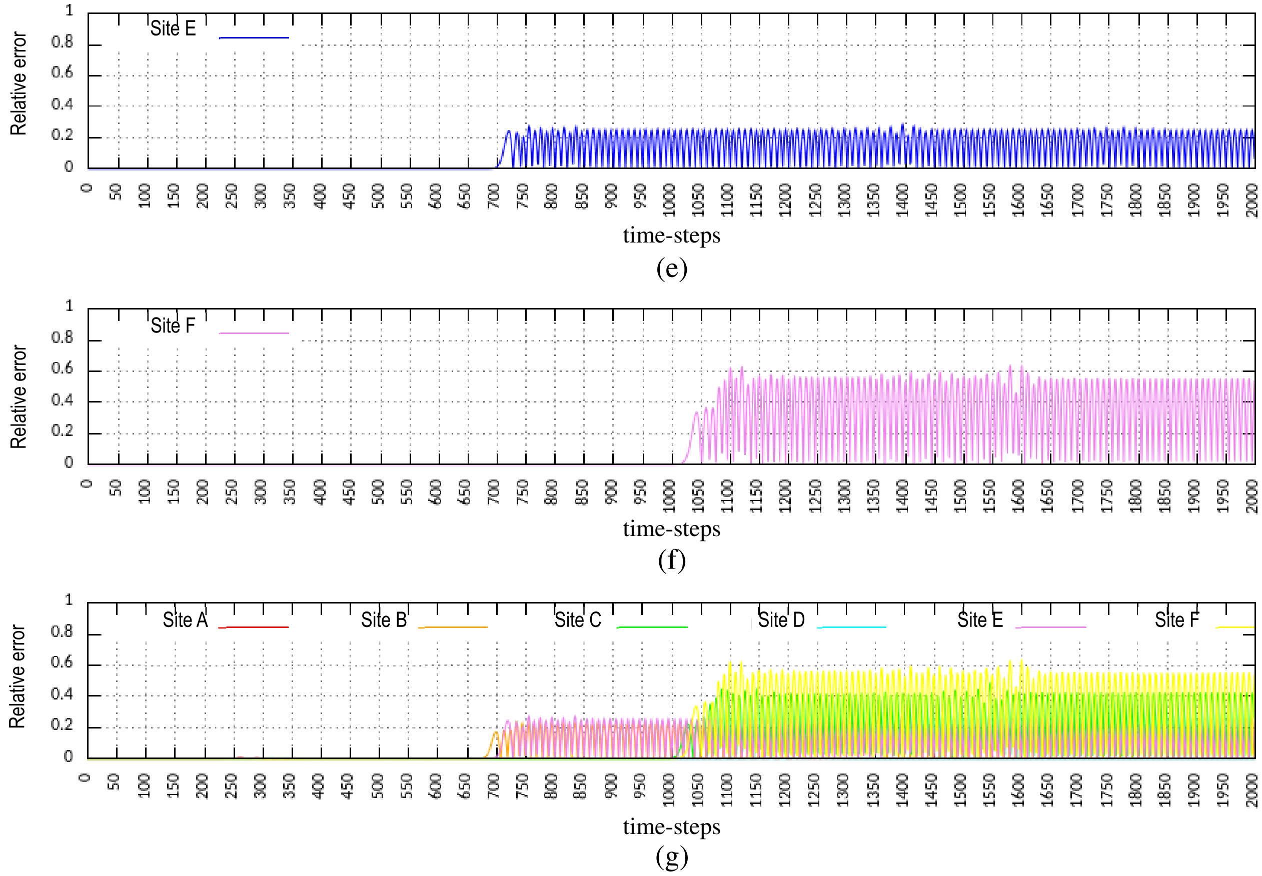

(e)

(f)

(g)

Figure 6. (a) Relative error at site A within 2000 time-steps using Perfectly Matched Layer. (b) Relative error at site B within 2000 time-steps using Perfectly Matched Layer. (c) Relative error at site C within 2000 time-steps using Perfectly Matched Layer. (d) Relative error at site D within 2000 time-steps using Perfectly Matched Layer. (e) Relative error at site E within 2000 time-steps using Perfectly Matched Layer. (f) Relative error at site F within 2000 time-steps using Perfectly Matched Layer. (g) Relative error at site F within 2000 time-steps using Perfectly Matched Layer.

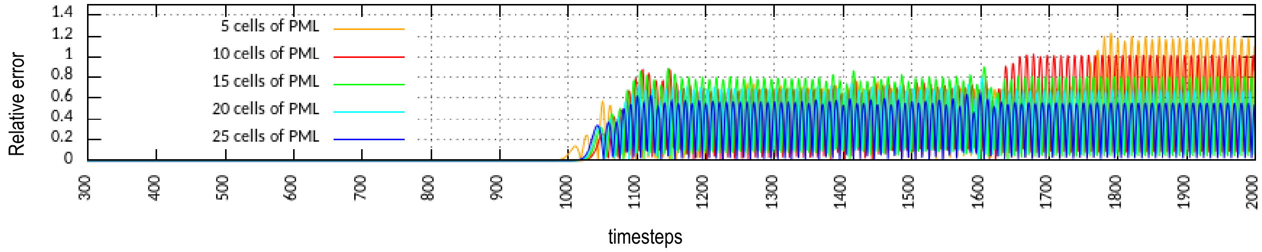

Figure 7. Relative errors at site F for 5, 10,15,20 and 25 PML cells at 2000-time steps.

experiments performed in this work. Ideally, the relative error must be suppressed to the greatest extent possible.

However, based on the numerical results obtained in this study, the upper limit of the largest relative error region is capped at 6×10^{-1}, which is excessively low in terms of efficiency. Nonetheless, assuming that the time steps in the FDTD simulation do not exceed $n_{\max} = 2000$, the errors in the simulated EM propagation are considered acceptable.

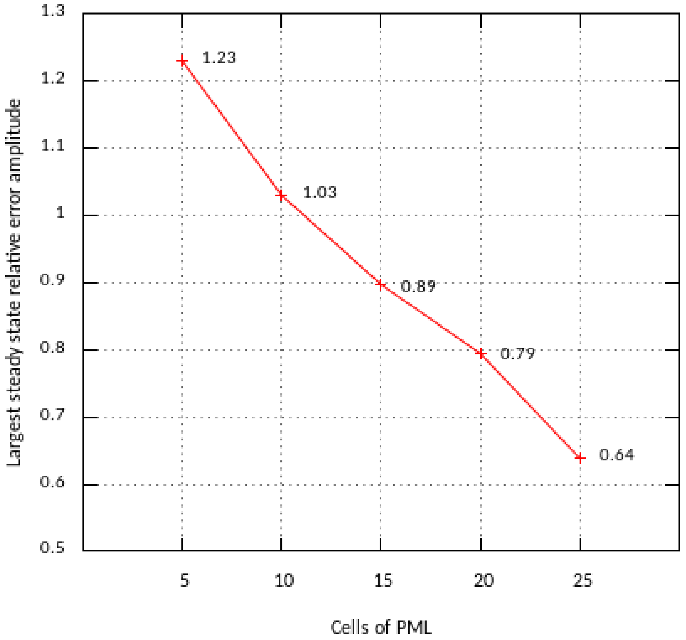

Figure 8. The values of relative error amplitude at a thickness $N_{\text{PML}} = 5, 10, 15, 20, 25$ in the PML implemented in the anisotropic ionospheric medium at site F.

Furthermore, to ensure that the errors obtained using the PML method are appropriately controlled for the preferred ABC method during the simulation of EM wave propagation in the ionosphere, an independent verification test on the efficiency of this FDTD code should be performed in future works.

4. CONCLUSIONS

In this work, numerical investigations were performed to evaluate the performance of two different types of ABCs: a differential ABC and the PML; these were implemented using FDTD code developed for dispersive, anisotropic media. The relative errors in the EM field were measured for both these methods, and the efficiency of the PML method was evaluated by varying its thickness, which cannot be performed for the differential ABC method. Furthermore, in terms of site-specific error reduction, the PML method was considered superior to the differential ABC method. This was determined by averaging the errors at all the other sites adopted in the experiments; notably, the overall relative error for the PML method was lower than that for the differential ABC method. In particular, the errors at certain sites were significantly suppressed under the PML approach, whereas site-specific suppression was not detected under the differential ABC approach. In addition, the highest steady-state relative error was reduced slightly on increasing the layer thickness, N_{PML}.

ACKNOWLEDGMENT

We thank the Ministry of Higher Education Malaysia for Fundamental Research Grant Scheme with Project Code: FRGS/1/2020/STG07/USM/03/3. The authors would like to extend their gratitude to Mr M. Musoddiq Jaafar for his assistance in preparing the manuscript and to Christopher Moore for reviewing the manuscript.

REFERENCES

1. Engquist, B. and A. Majda, "Absorbing boundary conditions for numerical simulation of waves," *Proc. Natl. Acad. Sci.*, Vol. 74, 1765–1766, 1977.

2. Mur, G., "Absorbing boundary conditions for the finite-difference approximation of the time-domain electromagnetic-field equations," *IEEE Trans. Electromagn. Compat.*, Vol. 23, 377–382, 1981.
3. Taflove, A., *Computational Electrodynamics: The Finite-Difference Time-Domain Method*, Artech House, 1995.
4. Berenger, J. P., "A perfectly matched layer for the absorption of electromagnetic waves," *J. Comput. Phys.*, Vol. 114, No. 2, 185–200, Oct. 1994, doi: 10.1006/jcph.1994.1159.
5. Yu, T. B., B. H. Zhou, and B. Chen, "An unsplit formulation of the Berenger's PML absorbing boundary condition for FDTD meshes," *IEEE Microw. Wirel. Components Lett.*, Vol. 13, 348–350, 2003.
6. Abdulkareem, B., J. P. Bérenger, F. Costen, R. Himeno, and H. Yokota, "An operator absorbing boundary condition for the absorption of electromagnetic waves in dispersive media," *IEEE Trans. Antennas Propag.*, Vol. 66, 2147–2150, 2018.
7. Chen, Y. and N. Feng, "Learning unsplit-field-based PML for the FDTD method by deep differentiable forest," *arXiv:2004.04815*, Jun. 16, 2021. [Online]. Available: http://arxiv.org/abs/2004.04815.
8. Tan, E. L., "A leapfrog scheme for complying-divergence implicit finite-difference time-domain method," *IEEE Antennas Wirel. Propag. Lett.*, Vol. 20, 853–857, 2021.
9. Valagiannopoulos, C. A. and N. K. Uzunoglu, "Rigorous analysis of a metallic circular post in a rectangular waveguide with step discontinuity of sidewalls," *IEEE Trans. Microw. Theory Tech.*, Vol. 55, No. 8, 1673–1684, Aug. 2007.
10. Sun, Y.-C., H. Ren, K. Yamazaki, et al., "Semi-analytical solutions of seismo-electromagnetic signals arising from the motional induction in 3-D multi-layered media: Part I — Theoretical formulations," *Earth, Planets and Space*, Vol. 73, No. 1, 1–26, 2021.
11. Bérenger, J. P., "An implicit FDTD scheme for the propagation of VLF-LF radio waves in the Earth-ionosphere waveguide," *Comptes Rendus Physique*, 2014.
12. Samimi, A. and J. J. Simpson, "Introducing a new method for FDTD modeling of electromagnetic wave propagation in magnetized plasma," *2014 USNC-URSI Radio Science Meeting (Joint with AP-S Symposium), USNC-URSI 2014 — Proceedings*, 158, Nov. 2014.
13. Fang, Y., X. L. Xi, J. M. Wu, J. F. Liu, and Y. R. Pu, "A J-E collocated WLP-FDTD model of wave propagation in isotropic cold plasma," *IEEE Trans. Microw. Theory Tech.*, Vol. 64, No. 7, Pt. 1, 1957–1965, 2016.
14. Pokhrel, S., J. J. Simpson, D. T. Welling, and M. W. Liemohn, "Regional FDTD modeling of GICs during the 2003 'Halloween' solar storm," *AGUFM*, Vol. 2018, IN33D-0884, Feb. 23, 2021. [Online]. Available: https://ui.adsabs.harvard.edu/abs/2018AGUFMIN33D0884P/abstract.
15. Pokhrel, S., V. Shankar, and J. J. Simpson, "Simplified FDTD model of electromagnetic wave propagation in magnetized plasma," *2018 International Applied Computational Electromagnetics Society Symposium (ACES)*, IEEE, Denver, CO, USA, May 2018.
    Smith, D. R., C. Y. Huang, E. Dao, S. Pokhrel, and J. J. Simpson, "FDTD modeling of high-frequency waves through ionospheric plasma irregularities," *J. Geophys. Res. Sp. Phys.*, Vol. 125, e2019JA027499, 2020.
16. Valagiannopoulos, C., "An overview of the Watson transformation presented through a simple example," *Progress In Electromagnetics Research*, Vol. 75, 137–152, 2007.
17. Li, M.-K. and W. C. Chew, "A new Sommerfeld-Watson transform in 3D," *IEEE Antennas and Propagation Society Symposium, 2004*, Vol. 2, IEEE, 2004.
18. Chen, Q., M. Katsurai, and P. H. Aoyagi, "An FDTD formulation for dispersive media using a current density," *IEEE Trans. Antennas Propag.*, Vol. 46, 1739–1746, 1998.
19. Yang, L., Y. Xie, and P. Yu, "Study of bandgap characteristics of 2D magnetoplasma photonic crystal by using M-FDTD method," *Microw. Opt. Technol. Lett.*, Vol. 53, 1778–1784, 2011.
20. Courant, R., K. Friedrichs, and H. Lewy, "On the partial difference equations of mathematical physics," *IBM J. Res. Dev.*, Vol. 11, 215–234, 1967.

21. Berenger, J. P., "Improved PML for the FDTD solution of wave-structure interaction problems," *IEEE Trans. Antennas Propag.*, Vol. 45, 466–473, 1997.
22. Yee, K., "Numerical solution of initial boundary value problems involving Maxwell's equations in isotropic media," *IEEE Trans. Antennas Propag.*, Vol. 14, No. 3, 302–307, 1966.
23. Rickard, Y. S. and N. K. Georgieva, "Problem-independent enhancement of PML ABC for the FDTD method," *IEEE Trans. Antennas Propag.*, Vol. 51, No. 10, 3002–3006, 2003.